

# 2D TRIPLE in orientationally disordered samples—a means to resolve and determine relative orientation of hyperfine tensors

D. Goldfarb,<sup>a,\*</sup> B. Epel,<sup>a</sup> H. Zimmermann,<sup>b</sup> and G. Jeschke<sup>c</sup>

<sup>a</sup> Department of Chemical Physics, Weizmann Institute of Science, Rehovot 76100, Israel

<sup>b</sup> Max-Planck Institute for Medical Research, Heidelberg, Germany

<sup>c</sup> Max-Planck Institute for Polymer Research, Mainz, Germany

Received 5 December 2003; revised 26 January 2004

## Abstract

The two-dimensional (2D) TRIPLE experiment provides correlations between electron-nuclear double resonance (ENDOR) frequencies that belong to the same electron-spin manifold,  $M_S$ , and therefore allows to assign ENDOR lines to their specific paramagnetic centers and  $M_S$  manifolds. This, in turn, also provides the relative signs of the hyperfine couplings. So far this experiment has been applied only to single crystals, where the cross-peaks in the 2D spectrum are well resolved with regular shapes. Here we introduce the application of the 2D TRIPLE experiment to orientationally disordered systems, where it can resolve overlapping powder patterns. Moreover, analysis of the shape of the cross-peaks shows that it is highly dependent on the relative orientation of the hyperfine tensors of the two nuclei contributing to this particular peak. This is done initially through a series of simulations and then demonstrated experimentally at a high field (W-band, 95 GHz). The first example concerned the  $^1\text{H}$  hyperfine tensors of the stable radical  $\alpha,\gamma$ -bis(diphenylene)- $\beta$ -phenylallyl (BDPA) immobilized in a polystyrene matrix. Then, the experiment was applied to a more complex system, a frozen solution of Cu(II)-bis(2,2':6',2''-terpyridine) complex. There, the 2D TRIPLE experiment was combined with the variable mixing time (VMT) ENDOR experiment, which determined the absolute sign of the hyperfine couplings involved, and orientation selective ENDOR experiments. Analysis of the three experiments gave the hyperfine tensors of a few coupled protons.

© 2004 Elsevier Inc. All rights reserved.

## 1. Introduction

Electron-nuclear double resonance (ENDOR) spectroscopy is a well established technique for recording the NMR spectrum of nuclei coupled to unpaired electron(s). In the pulse mode, ENDOR spectra are usually recorded using the Davies [1] or Mims [2] pulse sequences, which are currently applied routinely primarily at X-band frequencies, but also at Q-, W-, and D-bands (35, 95, and 140 GHz) [3–8]. Performing the ENDOR measurements at a high field has several advantages amongst which is the better resolution due to the increased nuclear Zeeman interaction. In addition, the ENDOR frequencies are often described by first order expressions and are therefore easier to analyze. This, in turn, results in hyperfine doublets which are symmetric

with respect to the nuclear Zeeman frequency such that the pulsed special TRIPLE experiment, which increases the ENDOR effect by up to a factor of 2, is applicable to solids as well as liquids [10]. Finally, better orientation selectivity is obtained for paramagnetic centers with anisotropic  $g$ -factors. These advantages have been demonstrated on paramagnetic transition metal sites in a variety of systems such as frozen solutions and single crystals of metalloproteins, metal substituted molecular sieves, and encapsulated complexes in zeolites [7,11–15].

Although the frequency ranges of many different types of nuclei are well apart at W-band, the problem of congested spectra, especially for protons still exists. This is particularly troublesome in orientationally disordered systems, where the spectrum is composed of a superposition of several overlapping powder patterns, with a number of singularities. In this case differentiating between singularities ascribed to powder line-shapes of the same proton, or to different protons is often difficult.

\* Corresponding author. Fax: +972-8-9344123.

E-mail address: [daniella.goldfarb@weizmann.ac.il](mailto:daniella.goldfarb@weizmann.ac.il) (D. Goldfarb).

Some of these problems can be alleviated by the application of a proper correlation spectroscopy, such as the two-dimensional (2D) TRIPLE experiment.

The TRIPLE experiment (also referred to as double ENDOR) was first designed in the continuous wave (CW) mode for determining the relative sign of the hyperfine coupling of different nuclei in a particular paramagnetic center [16,17]. The pulse mode analog of the TRIPLE experiment, shown in Fig. 1, was reported by Mehring et al. [18]. While the first RF pulse is set to one of the ENDOR transitions, the frequency of the second RF pulse is scanned to generate the TRIPLE spectrum. The difference between the resulting spectrum and the ENDOR spectrum yields the difference TRIPLE spectrum, which exhibits only ENDOR lines that belong to the same  $M_S$  manifold as the one selected by the first RF pulse. This experiment can be expanded to 2D by sweeping the frequencies of both RF pulses [19]. The latter technique is particularly useful when the spectrum is congested and consists of signals originating from different paramagnetic centers. The connectivities between the peaks in the 2D spectrum enable a straightforward assignment of the signals to their respective centers and  $M_S$  manifolds, thus providing the relative signs of hyperfine couplings. The feasibility and effectiveness of the experiment was demonstrated at W-band on a crystal of Cu(II) doped L-histidine. Homo-nuclear  $^1\text{H}$ - $^1\text{H}$ ,  $^{14}\text{N}/^{35}\text{Cl}$ - $^{14}\text{N}/^{35}\text{Cl}$  and hetero-nuclear  $^1\text{H}$ - $^{14}\text{N}/^{35}\text{Cl}$  2D TRIPLE spectra were recorded and from the various connectivities in the 2D map the  $^1\text{H}$ ,  $^{14}\text{N}$ , and  $^{35}\text{Cl}$  signals belonging to two different Cu(II) centers were identified and grouped according to their  $M_S$  manifolds [19].

Correlation spectroscopy on orientationally disordered systems is well known in NMR spectroscopy and characteristic cross-peak patterns have been identified and correlated with the geometry of the interaction [20,21]. This approach has been also applied to pulsed EPR in an experiment which correlates NMR frequencies of coupled nuclei with EPR frequencies [22]. Here we show that 2D TRIPLE correlation spectroscopy can unravel powder patterns of individual protons in orientationally disordered systems and provide relative orientations of hyperfine tensors. This is accomplished through the analysis of the unique line-shape of the

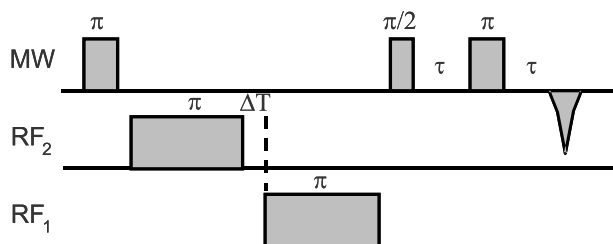


Fig. 1. The TRIPLE pulse sequence.

cross-peaks, initially demonstrated on a series of calculated 2D TRIPLE spectra followed by concrete examples. The first example involves a simple model, the radical BDPA ( $\alpha,\gamma$ -bis(diphenylene- $\beta$ -phenylallyl) immobilized in a polystyrene matrix and the second is a frozen solution of the Cu(II)-bis(2,2':6',2'' terpyridine) complex. In the latter, the 2D TRIPLE experiment was combined with the variable mixing time (VMT) ENDOR experiment [19], which provides the absolute sign of the hyperfine coupling, and a series of standard orientation selective ENDOR measurements.

## 2. Experimental

BDPA was purchased from Aldrich and the sample was prepared as described in [8]. The Cu(II)-bis(2,2':6',2'' terpyridine) complex with the ligand deuterated at positions 6 and 6'' was prepared as described in [25] and the Cu(II) concentration was 1 mM in a 1:1 ethanol:dichloromethane mixture (not degassed).

### 2.1. Spectroscopic measurements

All pulsed ENDOR and TRIPLE measurements were performed at W-band (94.9 GHz) on a home built spectrometer [7] at 5 and 20 K. The ENDOR probehead was similar to that described earlier [7] with typical RF  $\pi$ -pulses,  $t_{\text{RF}}$ , of 15–20  $\mu\text{s}$  for  $^1\text{H}$  (at 140 MHz). All reported ENDOR/TRIPLE measurements on the Cu(II) complex were carried out with MW  $\pi/2$  and  $\pi$  pulses,  $t_{\text{MW},\pi/2}$  and  $t_{\text{MW},\pi}$ , of 0.1 and 0.2  $\mu\text{s}$ , respectively,  $\tau$  delays of 0.35  $\mu\text{s}$  and repetition rates of 200 Hz. For BDPA the MW pulses were 0.15 and 0.3  $\mu\text{s}$ , respectively,  $\tau = 0.5 \mu\text{s}$  and the repetition rate was rather slow, 5 Hz, due to the long  $T_1$  at low temperature. The field-sweep echo-detected (FS-ED) EPR spectrum was recorded using a two-pulse echo sequence. Two-dimensional data sets had 150–160 points in each dimension. The delay,  $\Delta T$ , between the two RF pulses was 1  $\mu\text{s}$ . For each point in the 2D experiment 30–150 shots were averaged (1 scan). The VMT-ENDOR experiment is similar to the Davies ENDOR experiment, with an additional time delay, referred to as a mixing time,  $t_{\text{mix}}$ , inserted after the RF pulse, before the echo detection sequence [19].

### 2.2. Data manipulation

2D difference TRIPLE data were treated with Matlab software (The Math Works). Baseline correction was carried out for each slice in both dimensions and the value of the first data point in each slice was subtracted from the whole slice. This procedure yields the difference TRIPLE spectrum since the spectrum obtained by sweeping  $\text{RF}_2$  with  $\text{RF}_1$  off-resonance is equivalent to the normal ENDOR spectrum. Only the positive signals

are plotted. In the following we refer to difference TRIPLE spectrum simply as TRIPLE.

### 2.3. Simulations

Spectral simulations were carried out using a program developed in-house using Matlab. The ENDOR frequencies of the simple case of an electron spin,  $S = 1/2$ , coupled to  $n$ ,  $I = 1/2$  nuclear spins, are determined from the following Hamiltonian:

$$\hat{H} = \frac{\beta}{h} \vec{B} \cdot \mathbf{g} \cdot \hat{S} + \sum_{i=1}^n \left[ -\frac{g_{n,i} \beta_n}{h} \vec{B} \cdot \hat{I}_i + \hat{S} \cdot \mathbf{A}_i \cdot \hat{I}_i \right], \quad (1)$$

where the first and second terms describe the electron spin and nuclear spin Zeeman interactions, respectively, and the third term represents the hyperfine interaction. It is convenient to express  $\vec{B}$  and all the  $\mathbf{A}_i$ 's in the principal axis system of the  $\mathbf{g}$ -tensor ( $X, Y, Z$ ). Accordingly, the  $\mathbf{A}_i$ 's are characterized by their principal components,  $A_{xx,i}$ ,  $A_{yy,i}$ ,  $A_{zz,i}$  (or  $A_{||,i}$ , and  $A_{\perp,i}$  for an axially symmetric tensor) and the Euler angles  $\alpha_i$ ,  $\beta_i$ , and  $\gamma_i$  relating the  $\mathbf{A}_i$  principal axes system ( $x_i, y_i, z_i$ ) to that of the  $\mathbf{g}$  principal axes system. When  $\mathbf{g}$  is axially symmetric there is no dependence on  $\alpha_i$ , which can thus be set to zero. The anisotropic part of  $\mathbf{A}_i$  is represented by  $\mathbf{T}_i$ . The first order expression for the ENDOR frequencies for a weak coupling case, which usually holds for protons at high fields is

$$v_{\alpha,\beta,i} = v_I - M_S A_i, \quad (2)$$

where  $v_I = (g_n \beta_n)/hB_0$  is the nuclear Larmor frequency and  $A_i$  is a function of  $\beta_i$ ,  $\gamma_i$ , and the orientation of  $\vec{B}$  with respect to ( $X, Y, Z$ ), given by  $\theta_0$  and  $\phi_0$  [22]. For the case of an isotropic  $g$  the principal axes systems of the hyperfine tensors of the individual protons are given with respect to one arbitrarily chosen nucleus and are described by the angles  $\psi$  and  $\phi$ .

For an non-axially symmetric hyperfine interaction the powder pattern of each proton exhibits six singularities, given by:

$$\begin{aligned} v_{\alpha\alpha,i} &= v_I - \frac{1}{2} A_{xx,i}, & v_{\beta\alpha,i} &= v_I + \frac{1}{2} A_{xx,i}, \\ v_{\alpha\gamma,i} &= v_I - \frac{1}{2} A_{yy,i}, & v_{\beta\gamma,i} &= v_I + \frac{1}{2} A_{yy,i}, \\ v_{\alpha z,i} &= v_I - \frac{1}{2} A_{zz,i}, & v_{\beta z,i} &= v_I + \frac{1}{2} A_{zz,i}, \end{aligned} \quad (3)$$

whereas for an axial hyperfine interaction the singularities are denoted by  $v_{\alpha\perp,i}$ ,  $v_{\alpha\parallel,i}$ ,  $v_{\beta\perp,i}$ , and  $v_{\beta\parallel,i}$ .

The simulation program first calculates the ENDOR frequencies of the protons involved for a certain orientation of  $\vec{B}$  and then constructs the corresponding cross-peaks in the 2D TRIPLE spectrum that appear at  $(v_{\alpha_i}, v_{\alpha_j})$  and  $(v_{\beta_i}, v_{\beta_j})$  where the indices  $i$  and  $j$  assume all possible values between 1 and  $n$ . The cross-peak pattern is symmetric with respect to the exchange of the  $i$  and  $j$  indices and, in principle, it is sufficient to measure only

half of the spectrum. Nevertheless, for the sake of completeness and reassurance when weak cross-peaks are concerned, we measured the whole spectrum.

## 3. Results and discussion

### 3.1. Cross-peak shapes

The 2D TRIPLE spectrum shows on the diagonal the normal ENDOR spectrum, while the cross-peaks contain the correlation information. For a  $S = 1/2$ ,  $I_1 = 1/2$ ,  $I_2 = 1/2$  system, the pair of nuclei produces four cross-peaks, two for each  $M_S$  manifold. In orientationally disordered systems the shapes and positions of the cross-peaks are strongly dependent on the relative orientation and sign of the hyperfine tensors. This is illustrated in Fig. 2 which shows simulated 2D TRIPLE spectra for two protons and an isotropic  $g$ . In this case there is no orientation selectivity, namely, all possible orientations contribute to the spectrum, yielding a complete powder pattern. Furthermore, the only angle to be considered is that between the unique axes of the two hyperfine tensors  $z_1$  and  $z_2$ , given by  $\psi$ . The spectrum shown in Fig. 2A corresponds to the most simple example where the ENDOR powder patterns of the two protons do not overlap and the  $A_{||}$  and  $A_{\perp}$  singularities of each proton are clear and can be easily determined. Nonetheless, their relative orientation cannot be determined from the ENDOR spectrum. In this particular case  $\psi = 0^\circ$  and therefore the ridges appear as straight lines, ranging from  $(v_{||\alpha,1}, v_{||\alpha,2})$  to  $(v_{\perp\alpha,1}, v_{\perp\alpha,2})$  for the  $\alpha$ -manifold cross-peaks and from  $(v_{||\beta,1}, v_{||\beta,2})$  to  $(v_{\perp\beta,1}, v_{\perp\beta,2})$  for the  $\beta$ -manifold peaks (this specific peak is marked on the figure). In this case each slice of the 2D TRIPLE shows two well resolved Lorentzian (or Gaussian) lines. The projection of the cross-peaks onto the two different spectral axes,  $v_1$  and  $v_2$ , gives the extent of the powder pattern of each manifold. It is convenient to discuss the positions of the cross-peaks in terms of the four quadrants  $(+, +)$ ,  $(-, -)$ ,  $(+, -)$ , and  $(-, +)$ , where the sign gives the ENDOR frequency relative to  $v_I$ . In this particular case the complete cross-peaks are contained within the  $(+, +)$  and  $(-, -)$  quadrants, showing that for all orientations the hyperfine couplings of the two protons have the same sign.

The correlation ridges for  $\psi = 90^\circ$  are more complex, as shown in Fig. 2B, and have a shape of a right triangle, where the perpendicular edges reflect the width of the powder pattern of the individual protons given by  $|v_{||\alpha,\beta} - v_{\perp\alpha,\beta}|$ . Here, unlike for  $\psi = 0^\circ$ , in which each slice in the 2D spectrum consists of two well resolved peaks, the slices comprise partial powder patterns. For example  $v_{\perp\beta,1}$  correlates with all frequencies of  $v_{\beta,2}$  and vice-versa, and the corresponding slice looks like a powder pattern characteristic of an isotropic

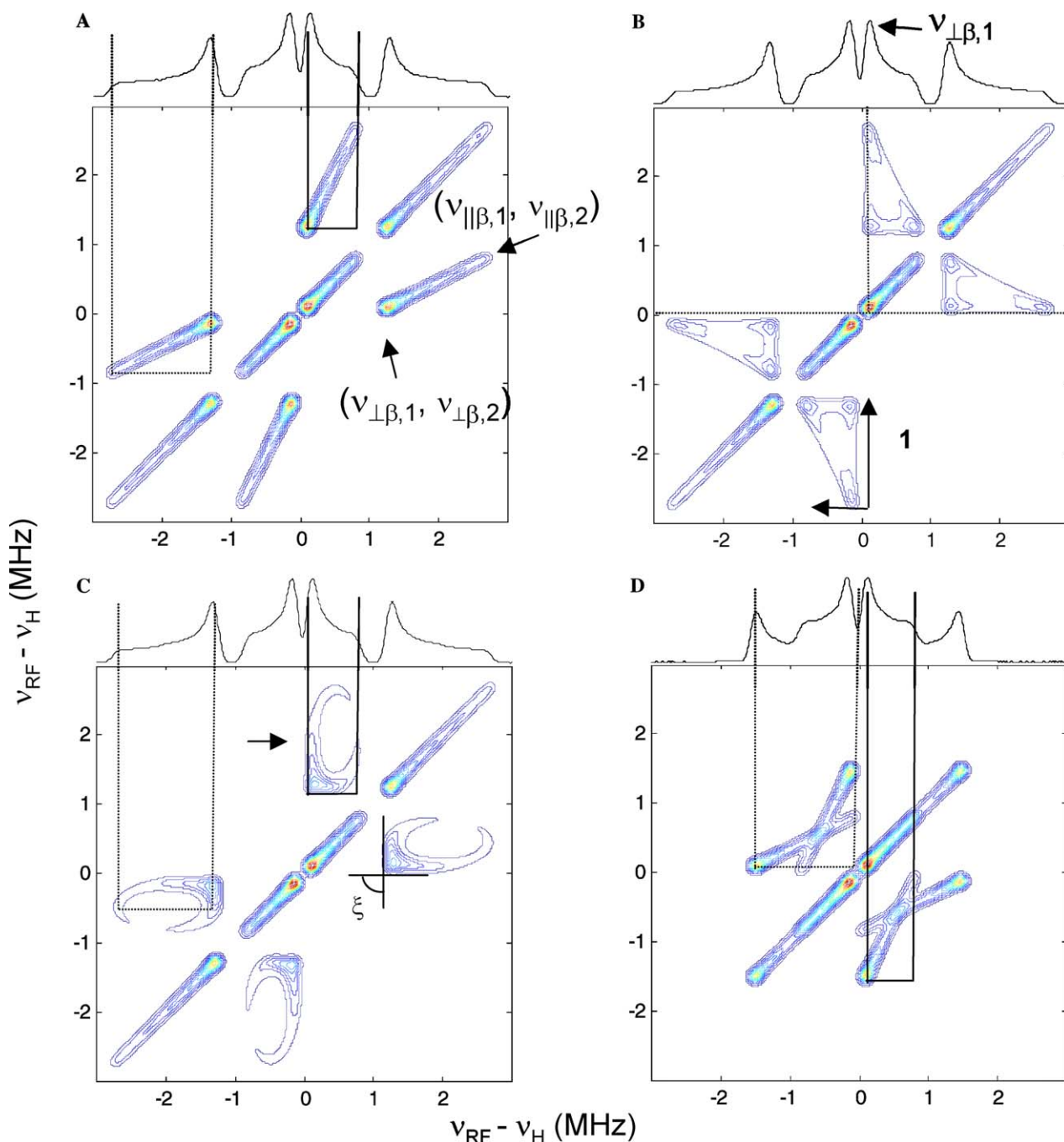


Fig. 2. Simulated 2D TRIPLE and ENDOR spectra ( $\theta_0 = 0-90^\circ$ ,  $\phi_0 = 0-180^\circ$ ) of two protons with (A)  $A_{\parallel}(1) = 1.7$  MHz,  $A_{\perp}(1) = 0.2$  MHz,  $A_{\parallel}(2) = 5.5$  MHz,  $A_{\perp}(2) = 2.5$  MHz,  $\psi = 0^\circ$ , (B) same but  $\psi = 45^\circ$ , (C) same but  $\psi = 90^\circ$ , (D)  $A_{\parallel}(1) = 1.7$  MHz,  $A_{\perp}(1) = 0.2$  MHz,  $A_{\parallel}(2) = -3$  MHz,  $A_{\perp}(2) = 0$  MHz,  $\psi = 0^\circ$ . The solid and dotted lines represent the projection of the cross-peaks on the ENDOR spectrum. For all other annotations see text. All spectra were calculated with a Lorentzian line width of 0.15 MHz.

distribution of orientations in a plane (see dotted lines in Fig. 2B). In fact, focusing on the cross-peak labeled “1” in Fig. 2B, it can be seen that the set of slices going up  $\rightarrow$  down are very similar to the line-shapes of a series of orientation selective ENDOR spectra of proton (1), for which  $z_1$  makes  $90^\circ$  with  $Z$  (see arrows). Similarly, the right  $\rightarrow$  left direction gives orientation selective ENDOR spectra for proton (2) [22]. The case of  $\psi = 45^\circ$

is shown in Fig. 2C. There, again, the projection of the cross-peak on each of the  $v_1$  and  $v_2$  axes gives the width of the corresponding powder pattern. Moreover, the position of the slice, which exhibits the broadest powder pattern within the cross-peak, gives an indication to the value of  $\psi$ , just as in orientation selective ENDOR spectra [23,24]. While for  $\psi = 90^\circ$  this position is at the edge of the cross-peak, for  $\psi = 45^\circ$  it is in the center (see

arrow on the figure). It is convenient to define the apex of the cross-peak by the angle  $\zeta$ , as noted on Fig. 2C. In the case of two axial tensors  $\zeta = 90^\circ$ , and both edges are parallel to the axes. Fig. 2D shows simulated 2D TRIPLE spectra for a case of overlapping powder patterns with  $\psi = 0^\circ$ . Here the position and shape of the cross-peaks immediately resolve the overlapping powder patterns, and  $v_{\parallel\alpha,\beta}$  and  $v_{\perp\alpha,\beta}$  can be readily identified, as noted by the dotted and solid lines.

Some typical cross-peak shapes involving non-axial hyperfine tensors are shown in Fig. 3. Fig. 3A shows an example of two protons with collinear tensors, where proton (1) has a non-axially symmetric hyperfine tensor, while proton (2) has an axial tensor. This is manifested in a broadening at one end of the cross-peak, lending the cross-peak a triangular shape. Since one of the tensors is axially symmetric, one of the edges of the triangle is parallel to the corresponding axis. Here a projection of the apexes of the cross-peaks onto the  $v_1$  and  $v_2$  axes corresponds to singularities of the ENDOR powder pattern, as depicted on the figure. When both tensors are non-axial, then none of the edges of the triangular cross-peaks is parallel to an axis, as shown in Fig. 3B. The case of two non-axial tensors with a relative orientation of  $\psi = 90^\circ$ ,  $\phi = 0^\circ$ , is shown in Fig. 3C. Again the projection of the apexes of the cross-peaks onto the axes provides the singularities of the ENDOR powder patterns. But, as compared to the axial case (Fig. 2D) none of the edges of the triangles is parallel to any of the axes. The case of  $\psi = 45^\circ$  is shown in Fig. 3D. Comparison of the cross-peak shape with that of the axial case (Fig. 2C) reveals, in principle, the same general shape but with  $\zeta \neq 90^\circ$  (none of the edges is parallel to the axes). Note, however, that when  $\psi < 45^\circ$ ,  $\zeta < 90^\circ$  also for an axial tensor (see Fig. 4). When one of the tensors is axial,  $\zeta \neq 90^\circ$  but one of the edges remains parallel to an axis.

The line-shape of the diagonal peaks is another important source of information because it is related to the number of chemically equivalent but geometrically inequivalent protons. If only one proton is present, then the width of the peak along the diagonal should be homogeneous, but when more than one proton is present, and  $\psi \neq 0^\circ, 180^\circ$ , then the shape of the cross-peak is a function of  $\psi$ . Fig. 4 shows the complete 2D TRIPLE spectrum of two protons with the same principal values and  $\psi = 90^\circ$ , along with a series of the spectra calculated for different  $\psi$ , showing only the  $(-, -)$  quadrant. For  $\psi = 0^\circ$  the diagonal is narrow since the cross-peaks fall on the diagonal. As  $\psi$  increases the diagonal broadens and assumes shapes with the same characteristics described above.

### 3.2. 2D TRIPLE of BDPA

BDPA is a stable radical that can serve as a good standard for ENDOR spectroscopy and as such it has

been studied by high field ENDOR at 140 GHz [8,9]. The structure of BDPA is given in Fig. 5, and the unpaired electron is delocalized over the two diphenylene rings with alternating spin density resulting in two groups of eight protons each with very similar hyperfine couplings within the groups [8,9]. The EPR spectrum, even at 140 GHz, is a nearly Gaussian line with a width of  $\sim 1$  mT. The  $^1\text{H}$  ENDOR spectrum of BDPA immobilized in a polystyrene matrix comprises two doublets; one with rather broad lines and a splitting of 5 MHz and the second with a splitting of 1.5 MHz. Simulations of this spectrum gave the following hyperfine couplings for the two types of protons:  $A_{xx,1} = 1.0$  MHz,  $A_{yy,1} = 1.0$  MHz,  $A_{zz,1} = 1.26$  MHz and  $A_{xx,2} = 7.7$  MHz,  $A_{yy,2} = 5.3$  MHz,  $A_{zz,2} = 2.2$  MHz [8]. The same parameters, scaled by  $\gamma_{\text{H}}/\gamma_{\text{D}}$ , were used to reproduce the  $^2\text{H}$  ENDOR spectrum of perdeuterated BDPA [9].

The 2D TRIPLE spectrum, shown in Fig. 5, exhibits as expected, four cross-peaks between the components of the two doublets. The cross-peaks are parallel to the  $v_1$  or  $v_2$  axis, showing that the anisotropy of the type 1 protons is very small and its total linewidth is  $\sim 1.7$  MHz. The width of the cross-peak in the other dimension,  $\sim 3$  MHz, provides the extent of the powder pattern of the type 2 protons, which has a large anisotropy. Moreover, the position of the cross-peaks shows that the couplings of protons 1 and 2 have different signs and therefore the hyperfine components of one of these protons should be taken as negative. The spectrum also shows that the diagonal peaks of type 2 protons have a shape of a square, confirming that there is more than one proton of this kind. Using the hyperfine values of type 2, and taking for simplicity two protons only, we calculated the cross-peak between them as a function of  $\psi$  and  $\phi$  (see Fig. 6). Comparison of the calculated spectra with the experimental results suggests that  $\psi = 60\text{--}90^\circ$ . The complete spectrum of BDPA was then simulated using one proton of type 1 and two of type 2 with  $\psi = 67^\circ$  as presented in Fig. 6. The shape of the diagonal peak of the type 1 protons was not clear enough to try and reproduce it since it also overlaps with the signals of distant protons appearing at the  $^1\text{H}$  Larmor frequency. These produce “cross-like” cross-peaks on the diagonal due to correlations with the signals of type 1 protons. The correlation of the matrix line with type 2 protons can be recognized as well. Some of the cross-peaks with the distant protons are marked with dotted ellipses in Fig. 5.

### 3.3. Cu(II)-bis(2,2':6',2'' terpyridine) complex

In this part we present a strategy to resolve proton couplings in the Cu(II)-bis(terpyridine) complex, to determine the principal components of their hyperfine interaction, their absolute signs and their orientation with respect to  $\mathbf{g}$ . This was done by a combination of 2D

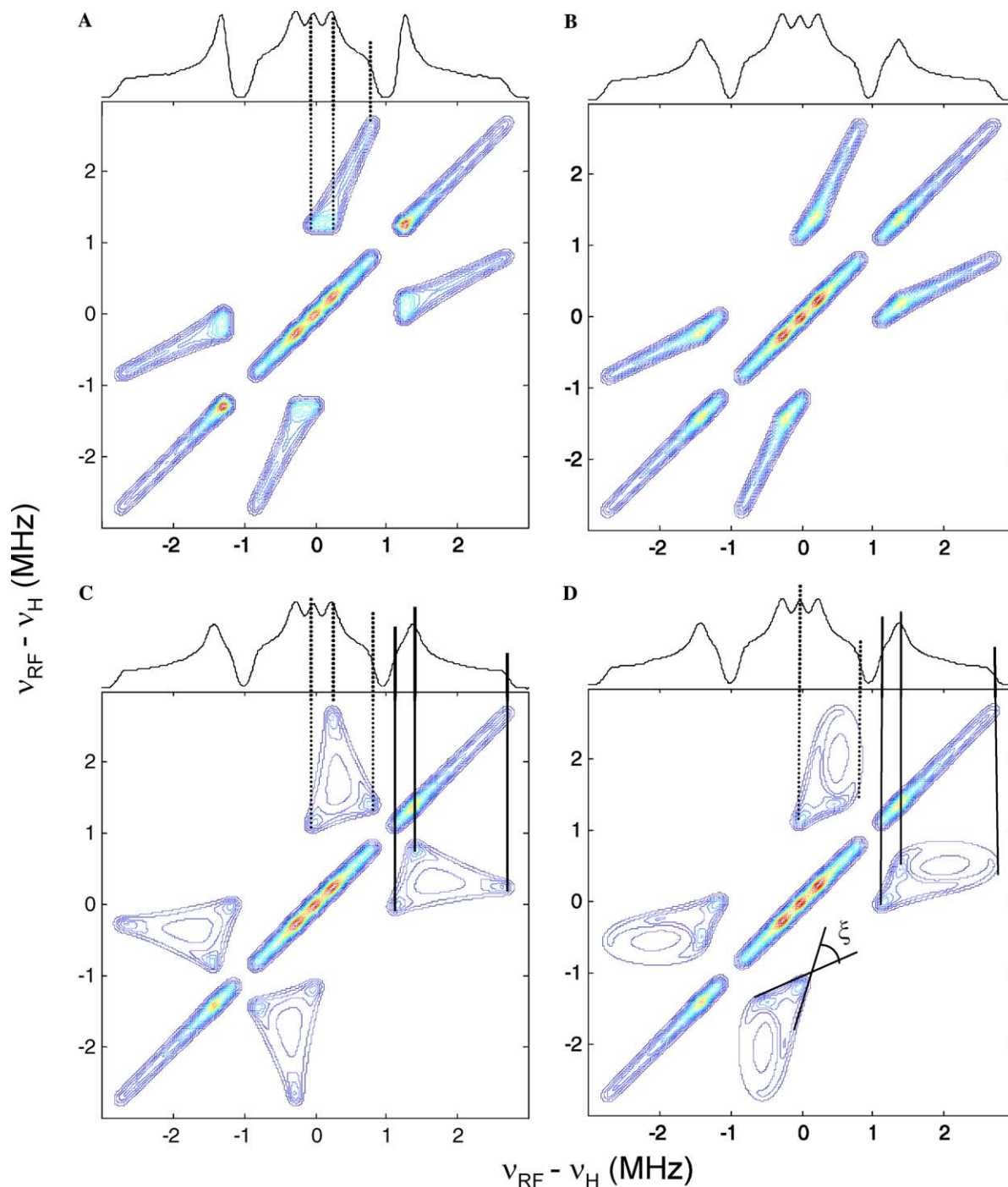


Fig. 3. Simulated 2D TRIPLE and ENDOR spectra ( $\theta_0 = 0-90^\circ$ ,  $\phi_0 = 0-180^\circ$ ) of two protons with (A)  $A_{zz}(1) = 1.7$  MHz,  $A_{yy}(1) = -0.1$  MHz,  $A_{xx}(1) = 0.3$  MHz,  $A_{||}(2) = 5.5$  MHz,  $A_{\perp}(2) = 2.5$  MHz,  $\psi = 0^\circ$ ,  $\phi = 0^\circ$ . (B)  $A_{zz}(1) = 1.7$  MHz,  $A_{yy}(1) = -0.1$  MHz,  $A_{xx}(1) = 0.3$  MHz,  $A_{zz}(2) = 5.5$  MHz,  $A_{yy}(2) = 2.2$  MHz,  $A_{xx}(2) = 2.8$  MHz,  $\psi = 0^\circ$ ,  $\phi = 0^\circ$ . (C) Same as (B) but  $\psi = 90^\circ$ ,  $\phi = 0^\circ$  (D) same as (B) but  $\psi = 45^\circ$ ,  $\phi = 0^\circ$ . The solid and dotted lines represent the projection of the ENDOR spectrum singularities. For all other annotations please see text. All spectra were calculated with a Lorentzian line width of 0.15 MHz.

TRIPLE, orientation-selective ENDOR, and VMT-ENDOR. Fig. 7 shows the structure of the complex as predicted from DFT (density functional theory) calculations, along with the calculated principal axis system of  $\mathbf{g}$  and the notation used for the various protons [25]. The Cu(II) is coordinated to two tridentate ligands, re-

ferred to as I and II, each having three pyridine rings. The center pyridine ring has two types of protons (4' and 3' and 5') whereas the two outer rings have four types of protons as noted on Fig. 7. The ligand used in this study was deuterated in positions 6 and 6'' and Table 1 lists Cu–H distances for all the other protons in the

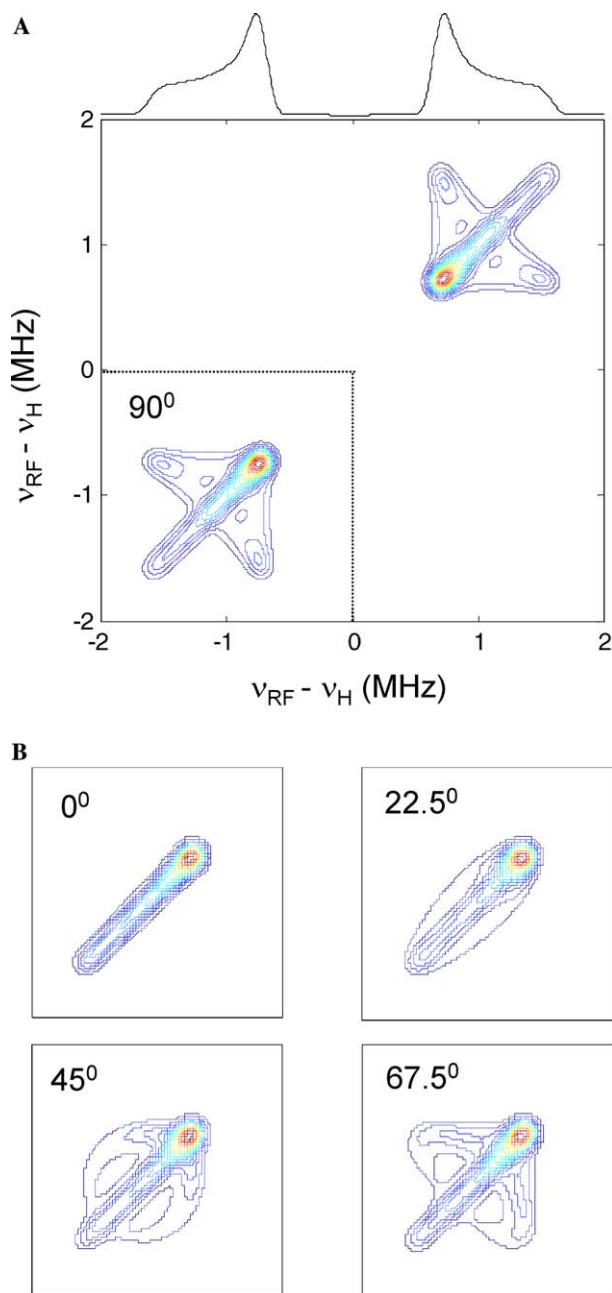


Fig. 4. Simulated 2D TRIPLE spectra ( $\theta_0 = 0\text{--}90^\circ$ ,  $\phi_0 = 0\text{--}180^\circ$ ) for two equivalent protons with (A)  $A_{\parallel} = 3.2\text{ MHz}$ ,  $A_{\perp} = 1.4\text{ MHz}$ , and  $\psi = 90^\circ$ , (B) same, showing only the  $(-, -)$  quadrant for different values of  $\psi$ . (All spectra were calculated with a Lorentzian line width of  $0.15\text{ MHz}$ .)

Cu(II)-terpyridine complex the structure of which was determined from DFT calculations [25].

Earlier X-band CW EPR measurements of the complex in different solvents showed that the  $g$ -values are slightly dependent on the solvent, specifically the difference between  $g_{xx}$  and  $g_{yy}$ . For example, the EPR parameters in ethanol were:  $g_{xx} = 2.028$ ,  $g_{yy} = 2.096$ ,  $g_{zz} = 2.260$ ,  $A_{\perp}(\text{Cu}) = 2\text{ mT}$ , and  $A_{\parallel}(\text{Cu}) = 15.8\text{ mT}$ , while in a 1:1 mixture of ethanol and dichlorome-

thane the difference between  $g_{xx}$  and  $g_{yy}$  is significantly reduced (see below) [25]. Earlier X-band  $^{14}\text{N}$  and W-band  $^2\text{H}$  ENDOR measurements on this complex showed that the nuclei on ligands I and II are not equivalent. In fact, this is expected due to the Jahn–Teller distortion of the complex. One ligand contributes three nitrogen lone pairs to the overlap with the  $3d_{x^2-y^2}$  orbital of the copper ion (equatorial positions). The other ligand contributes only one lone pair to this overlap, while the other two nitrogen lone pairs are involved in the much weaker and less well defined coordination to the axial positions. The  $^2\text{H}$  ENDOR orientation selective spectra could be very well reproduced with one type of deuterons, assigned to ligand I. The absence of clear features due to deuterons II6 and II6'' was attributed to a weaker coupling and broadening due to a large distribution in the Cu–N distances of the nitrogens in the outer rings of ligand II. Differences between ligands I and II were also predicted by DFT calculations [25].

Fig. 8A shows the W-band FS-ED EPR spectrum of the complex in a 1:1 mixture of ethanol and dichloromethane. Simulation of the spectrum gave  $g_{xx} = 2.056$ ,  $g_{yy} = 2.066$ , and  $g_{zz} = 2.249$ . A series of VMT-ENDOR spectra, recorded at the field position ( $g_{yy}$ ) denoted by an arrow in Fig. 8A, are shown in Fig. 8B. At a short  $t_{\text{mix}}$  the spectrum exhibits three major resolved doublets with splittings of 3.6, 2.6, and 1.9 MHz, which we label as  $a$ ,  $b$ , and  $c$ , respectively. In addition, it has a signal at  $\nu_{\text{H}}$  and a weak doublet with a small splitting of  $\sim 1\text{ MHz}$ , referred to as  $d$ . As  $t_{\text{mix}}$  increases, the intensity of the low frequency components of the  $a$ ,  $b$ , and  $c$  doublets is reduced considerably. This assigns the low frequency components to the  $\alpha$ -manifold and using Eq. (2) this yields a positive value for three hyperfine couplings. In contrast, it seems that the high frequency component of doublet  $d$  is reduced with  $t_{\text{mix}}$ , thus suggesting that its hyperfine coupling is negative.

The 2D TRIPLE spectrum, recorded at  $g_{yy}$  and presented in Fig. 9A, consists of cross-peaks between all components of the three doublets, namely  $(a, b)$ ,  $(a, c)$ , and  $(b, c)$ , all concentrated in the lower left  $(-, -)$  and upper right  $(+, +)$  quadrants. This confirms the results of the VMT-ENDOR experiments that all couplings have the same sign. The position and extent of the cross-peaks show that the width of the individual powder patterns is small. While the cross-peaks involving signal  $c$  are rather narrow, the ridge of the  $(a, b)$  cross-peaks extends from  $\pm 1.3$  to at least  $\pm 1.8\text{ MHz}$  for signal  $a$  and from  $\pm 1.05$  to at least  $\pm 1.3\text{ MHz}$  for signal  $b$ . In addition to these, cross-peaks between each of the  $a$ ,  $b$ , and  $c$  doublet components and the central signal appear parallel/perpendicular to the axes, revealing the width of the central signal. Their small width in one of the dimensions indicates again a small width of the powder patterns involving signal  $a$ ,  $b$ , and  $c$ . Interestingly, these ridges are not symmetric with respect to the zero

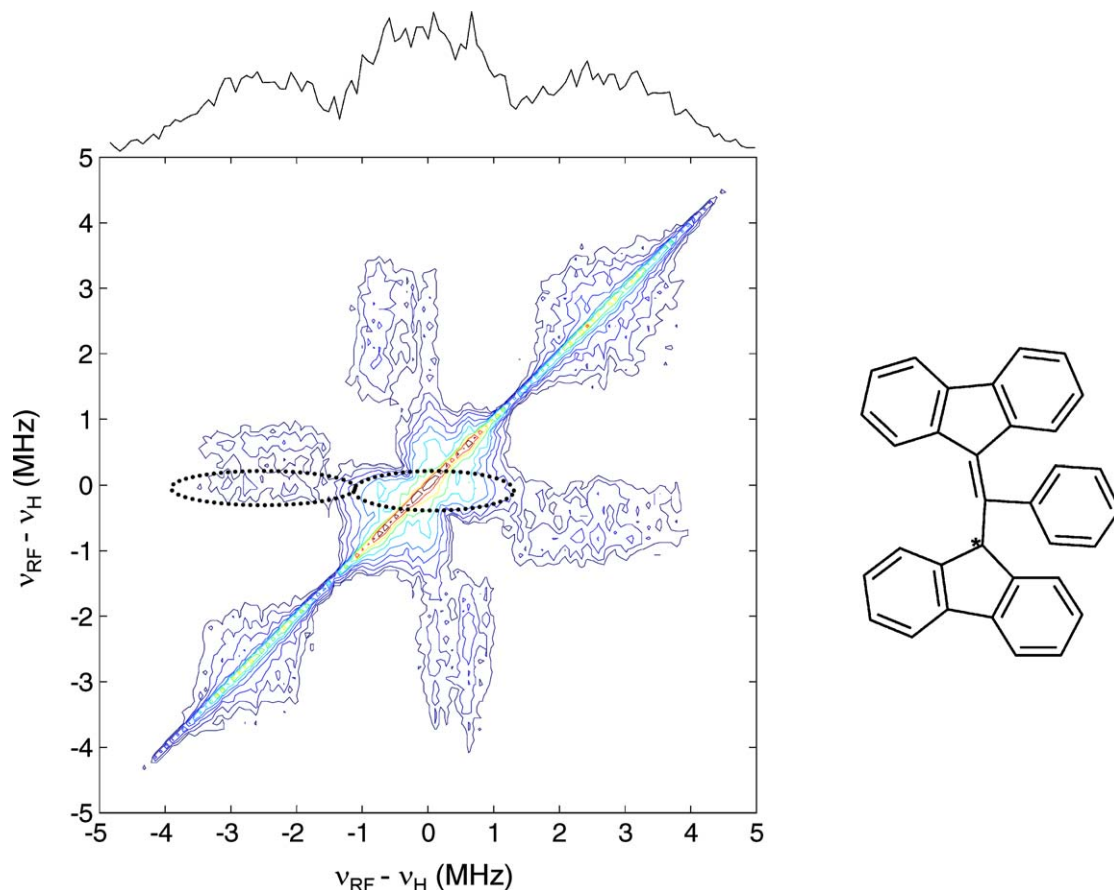


Fig. 5. The BDPA radical and its 2D  $^1\text{H}$  TRIPLE spectrum recorded at 20 K. The dotted ellipses represent cross-peaks with the matrix line.

frequency and are most probably due to superposition of a cross-peak with the matrix line and one of the components of the *d* doublet. In agreement with the VMT results, this yields a negative sign for the hyperfine coupling of signal *d* because the correlated peaks are on different sides of the Larmor frequency. Finally, there is a “cross-like” cross-peak in the center of the spectrum which we assign to a cross-peak between *d* and the matrix line, similar to that observed for BDPA (see Fig. 5).

The 2D TRIPLE spectrum suggests that signals *a*, *b*, and *c* can be due to three different protons with small anisotropies, alternatively, that they can arise from only two protons, each exhibiting more than one singularity. To resolve this uncertainty and further assign the *a*, *b*, and *c* peaks to specific singularities, orientation-selective Davies ENDOR spectra were collected along the EPR powder pattern. The spectra, presented in Fig. 10, show that the maximum splitting of doublets *a* and *b* (3.6 and 2.6 MHz, respectively) appears close to  $g_{yy}$ . When  $B_0$  decreases towards  $g_{zz}$ , both splittings decrease and merge. In contrast, doublet *c* exhibits a very subtle orientation dependence, it changes from 1.9 MHz at  $g_{yy}$  to 1.7 MHz at  $g_{zz}$ , where it merges with the *a* and *b* signals. The single resolved doublet observed at  $g_{zz}$  is superimposed on a broad background with a maximum splitting

of  $\sim 3.6$  MHz. The behavior of doublets *a* and *b*, namely increasing coupling as  $g_{zz} \rightarrow g_{yy}$ , indicates that the *a* signal at  $g_{zz}$  corresponds to  $v_{\perp}$ , and to  $v_{\parallel}$  at  $g_{yy}$  and therefore  $\beta \sim 90^\circ$ . In this case  $v_{\perp}$  should be observed also at  $g_{yy}$ . Hence, it must overlap with the *b* or *c* signals. The same arguments hold for doublet *b*, which exhibits a similar behavior, just with a smaller coupling. An alternative assignment is that the *a* signal at  $g_{zz}$  corresponds to  $v_{\parallel}$ , while at  $g_{yy}$  it corresponds to  $v_{\perp}$  and  $\beta = 0^\circ$ . This is, however, unlikely, because the condition  $v_{\perp} > v_{\parallel}$  under the constraint of a positive total coupling (as determined from the VMT-ENDOR) would imply a negative  $T_{zz}$  value. This is unexpected because the point-dipole approximation, which should be fairly good in this case, predicts a positive value. Moreover, our previous DFT computation also predicts positive  $T_{zz}$  values for all protons [25]. Therefore, we conclude that  $\beta \sim 90^\circ$  for the protons exhibiting signals *a* and *b*, and therefore they must originate from ligand I (see Table 1).

For all protons in ligand I the angle between the Cu–H and the  $g_{zz}$  directions is close to  $90^\circ$  as determined from the DFT structure shown in Fig. 7. Moreover, the presence of a number of protons with the same orientation will enhance the ENDOR signal. This suggests that the differences between the hyperfine couplings of



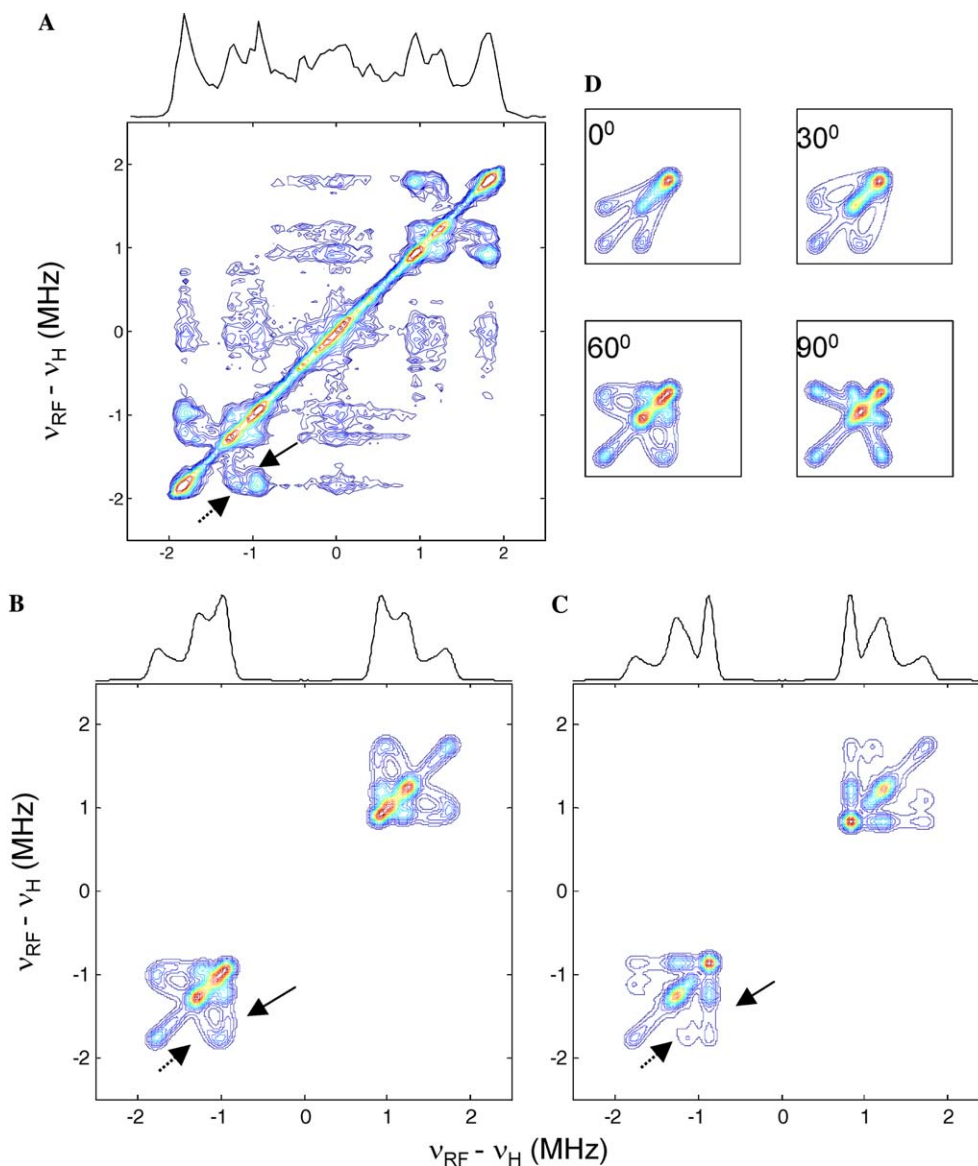


Fig. 9. (A) W-band  $^1\text{H}$  2D TRIPLE spectrum of a frozen solution of  $\text{Cu}(\text{II})$ -bis(2,2':6',2'' terpyridine) recorded at 6 K and  $g_{yy}$ . (B) Simulated spectra with two protons (parameter set A in Table 2). (C) Simulated spectra with three protons (parameter set B in Table 2). For all calculated spectra  $\theta_0 = 80$ – $90^\circ$ ,  $\phi_0 = 0$ – $180^\circ$  and the line-width was 0.15 MHz. (D) same as (C) showing only the  $(-, -)$  quadrant for different  $|\gamma_1 - \gamma_2|$  values.

Spectra measured beyond  $g_{yy}$ , towards  $g_{xx}$  at higher magnetic fields, exhibit a decrease in the splitting of  $a$  and a slight increase of  $c$ . This is attributed to some selectivity in  $\phi_0$  in this region due to the presence of a slight, unresolved non-axiality in  $\mathbf{g}$ . This is in contrast to the region between  $g_{zz}$  and  $g_{yy}$  where  $\phi_0$  assumes practically all possible orientations. The selectivity in  $\phi_0$  results in a decrease in the maximum splitting for  $\gamma \sim 0^\circ$ , while for  $\gamma \sim 90^\circ$  it increases the minimum splitting, both these trends are observed for the top three spectra. Taking this into account, the orientation selective ENDOR spectra (not including doublet  $d$  and the matrix line) could be reasonably reproduced (Fig. 10, left column) using two protons, noted by  $x_1$  and  $x_2$ , with close to axially symmetric hyperfine tensors as listed in Table 2 under set A

(the values of  $\gamma$  were refined based on the simulations of the 2D TRIPLE given below). Simulations carried out with three protons, called  $y_1$ ,  $y_2$ , and  $y_3$ , represented by set B in Table 2, are shown in the right column of Fig. 10. For both cases the signal intensity of signal  $c$  is too high in the calculated spectra. This is partially attributed to the reduced sensitivity of the Davies ENDOR experiment to small couplings. For a  $\text{MW}\pi$  pulse of 0.2  $\mu\text{s}$ , as used in the TRIPLE measurements, the relative intensities of three doublets of 1.7, 2.6, and 3.6 MHz, after taking the hyperfine contrast factor into account [26] is 0.78, 0.95 and 1.0, respectively. Comparison of the two sets of simulated spectra with the experimental one shows that the relative intensities for set A with two protons reproduce the experimental results better.

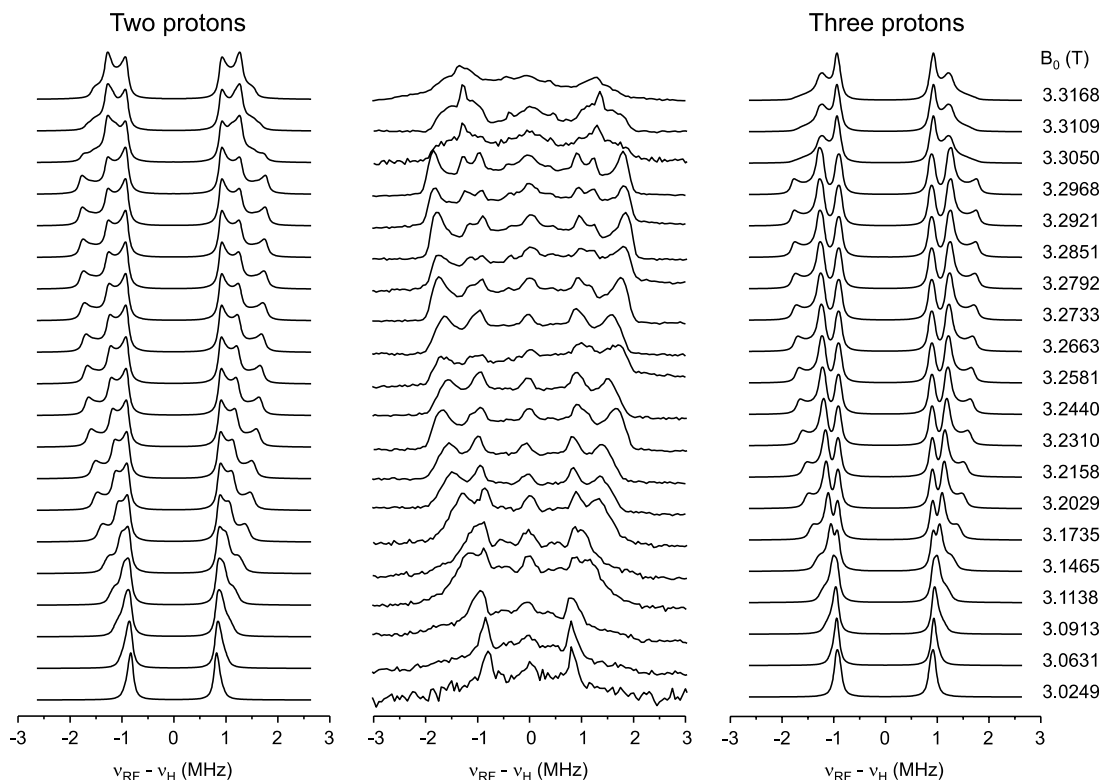


Fig. 10. Orientation selective  $^1\text{H}$  Davies ENDOR of the Cu(II)-bis(2,2':6',2'' terpyridine) complex. Magnetic field values  $B_0$  corresponding to the spectra are noted on the right. The center column shows series of experimental spectra recorded at 6 K. Simulated spectra with two protons (parameter set A in Table 2) are shown on the left and simulated spectra with three protons (parameter set B in Table 2) on the right. The following selected orientations were taken for all simulations (bottom to top)  $\theta_0 = 0-25^\circ, 20-30^\circ, 28-37^\circ, 34-42^\circ, 40-48^\circ, 48-54^\circ, 54-60^\circ, 56-62^\circ, 62-68^\circ, 66-72^\circ, 68-74^\circ, 70-78^\circ, 72-85^\circ, 74-90^\circ, 77-90^\circ, 80-90^\circ, 83-90^\circ, 85-90^\circ, 85-90^\circ,$  and  $85-90^\circ$ . For the top three spectra  $\phi_0 = 0-140^\circ, 0-130^\circ,$  and  $0-120^\circ$  (from bottom to top), otherwise  $\phi_0 = 0-180^\circ$ .

Table 1

The Cu–H distances for the various protons in Cu(II)-bis(2,2':6',2'' terpyridine) and their orientations with respect to the  $\mathbf{g}$  principal axis system as determined from the DFT calculated structure[25], along with the  $T_{zz}$  value obtained from the point-dipole approximation

Proton	Cu–H distance (Å)	$\beta$ (deg)	$\gamma$ (deg)	$T_{zz}$ (MHz)
I3	5.11	86.8	129.8	1.18
I3'	5.06	89.2	154.8	1.21
I3''	5.11	93.2	-129.8	1.18
I4	6.01	85.3	105.6	0.72
I4'	5.82	90.0	180.0	0.80
I4''	6.01	94.7	-105.6	0.72
I5	5.30	85.1	80.7	1.06
I5'	5.06	90.8	-154.8	1.21
I5''	5.30	94.9	-80.7	1.06
II3	5.25	42.6	-1.3	1.10
II3'	5.13	65.3	0.3	1.16
II3''	5.25	137.4	1.3	1.10
II4	6.21	19.6	-3.7	0.66
II4'	5.92	90.0	0.0	0.76
II4''	6.21	160.4	3.7	0.66
II5	5.53	4.5	169.8	0.94
II5'	5.13	114.7	-0.3	1.16
II5''	5.53	175.5	169.8	0.94

The 2D TRIPLE spectra were simulated using both sets of parameters, A and B, listed in Table 2 and the spectra are shown in Figs. 9B and C. While we know from the orientation selective ENDOR spectra that  $\beta \sim 90^\circ$  for all protons,  $\gamma$  was determined by the position and shape of the  $(a, b)$  cross-peak. Fig. 9D presents the dependence of the shape of the cross-peak in the  $(-, -)$  quadrant on  $\gamma$  for  $\beta_1 = \beta_2 = 90^\circ$  and a selected range of orientations of  $\theta_0 = 80-90^\circ$  using the parameters of set B. These show that the experimental spectrum is closest to the  $|\gamma_1 - \gamma_2| \sim 60^\circ$  spectrum. While the experimental spectrum does not show a full ridge for the  $(a, c)$  peak, both simulated spectra do, although with a reduced intensity in its central part (see solid arrows in Figs. 9B and C). This difference can be attributed to signal-to-noise ratio limitations. The intensities of the experimental spectra are better reproduced by the simulation with only two protons (set A). For example, the full ridge of the  $(a, b)$  peak is reproduced in the two-protons spectra (see dotted arrows in Figs. 9B and C) but not in the three-proton spectrum. On the other hand, in the latter the resolved  $(a, c)$  and  $(a, b)$  peaks (see arrows in Fig. 9A) are closer to the experimental results.

For simplicity, in these simulations we took into account only one proton for each type of protons con-

Table 2

The hyperfine parameters used to simulate the 2D TRIPLE and orientation selective ENDOR spectra

Proton	$A_{xx}$ (MHz)	$A_{yy}$ (MHz)	$A_{zz}$ (MHz)	$\beta$ (deg)	$\gamma$ (deg)
set A, x1	1.6	1.8	3.6	90	30
set A, x2	1.6	1.8	2.6	90	90
set B, y1	1.7	2.4	3.6	90	30
set B, y2	1.7	2.1	2.6	90	90
set B, y3	1.7	1.7	1.7	0	0

tributing to the spectrum and did not attempt to reproduce the shape of the diagonal peaks, although it is clear from the complex structure that several protons of ligand I are represented by protons  $x1$  and  $x2$  in set A, and  $y1$ ,  $y2$ , and  $y3$  in set B. We also did not attempt to simulate the cross-peaks with the central signal because it involves many different distant nuclei that cannot be reasonably assigned. Nonetheless, for both sets A and B the cross-peak should be broader than what is observed in the experimental spectra, and is expected to fill all the space covering the  $a$ – $c$  range. This can again be attributed to the  $S/N$  since the signal between peaks  $a$  and  $c$  is low.

Taking into consideration the 2D TRIPLE and the orientation selective ENDOR results, set A with two protons seems to reproduce the experimental results better. Further assignment of the two protons to specific protons in the complex can be obtained by comparison of the experimentally determined anisotropic hyperfine couplings with the  $T_{zz}$  calculated from the DFT structure using the point-dipole approximation given in Table 1. In ligand I for protons, I3, I3', I5', and I3''  $T_{zz} \sim 1.2$  MHz, for protons I5 and I5',  $T_{zz} \sim 1.1$  MHz and for I4, I4', and I4''  $T_{zz} \sim 0.7$ – $0.8$  MHz. The experimental  $T_{zz}$  values for the two protons are 1.0 and 0.4 MHz, respectively. Accordingly, we assign  $x1$  to the six protons I3, I3', I3'', I5, I5', and I5'', which are not resolved, and  $x2$  to the three I4, I4', and I4'' protons. Taking the relative numbers of protons in each group into account should lead to an increase in signal  $a$  relative to  $b$  in the simulated orientation selective spectra (Fig. 10, left column) and improves the agreement with the experimental spectra. Doublet  $d$  could arise from protons of ligand II.

#### 4. Summary and conclusions

We have demonstrated that the 2D TRIPLE correlation experiment can resolve overlapping powder patterns in orientationally disordered systems. Moreover, each cross-peak contains detailed information on the hyperfine tensors of a pair of nuclei; its shape reflects the anisotropy of each tensor and the relative orientation of the two tensors. The main disadvantage of the experiment is the low sensitivity since it is a double “differ-

ence” experiment and therefore it usually requires long accumulation times. In principle, this is not a problem if the experiment can be run at room temperature, where a stable operation of the spectrometer over days can be achieved. For low temperature measurements, such extensive averaging may be more difficult, although overnight experiments are already becoming standard. Another difficulty may arise from the fact that each pair of ENDOR transitions produces two cross-peaks, so that in the case of  $I = 1/2$  nuclei, like protons, the number of cross-peaks increases like  $4(n-1)!$  and spectra can easily become congested. Nonetheless, it is sufficient to have one nucleus with resolved signals in the ENDOR spectrum and the correlation peaks of this nucleus will actually resolve the whole spectrum.

#### Acknowledgments

This research was supported by the DFG Schwerpunkt program “High field EPR in Physics, Chemistry and Biology.”

#### References

- [1] E.R. Davies, A new pulse ENDOR technique, Phys. Lett. 47A (1974) 1–2.
- [2] W.B. Mims, Pulsed ENDOR experiments, Proc. R. Soc. London A 283 (1965) 452–457.
- [3] C.E. Davoust, P.E. Doan, B.M. Hoffman, Q-band pulsed electron spin-echo spectrometer and its application to ENDOR and ESEEM, J. Magn. Reson. A 119 (1996) 38–44.
- [4] I. Gromov, J. Shane, J. Forrer, R. Rakhmatoullin, Y. Rozentzwaig, A. Schweiger, A Q-band pulse EPR/ENDOR spectrometer and the implementation of advanced one- and two-dimensional pulse EPR methodology, J. Magn. Reson. 149 (2001) 196–203.
- [5] J.A.J.M. Disselhorst, H. Vandermeer, O.G. Poluektov, J. Schmidt, A pulsed EPR and ENDOR spectrometer operating at 95 GHz, J. Magn. Reson. 115 (1995) 83–188.
- [6] T.F. Prisner, M. Rohrer, K. Möbius, Pulsed 95 GHz high-field EPR heterodyne spectrometer with high spectral and time resolution, J. Magn. Reson. 7 (1994) 167–183.
- [7] I. Gromov, V. Krymov, P. Manikandan, D. Arieli, D. Goldfarb, A W-band pulsed ENDOR spectrometer: setup and application to transition metal centers, J. Magn. Reson. 139 (1999) 8–17.
- [8] M. Bennati, C.T. Farrar, J.A. Bryant, S.J. Inati, V. Weis, G. Gerfen, P. Riggs-Gelasco, J. Stubbe, R.G. Griffin, Pulsed electron-nuclear double resonance (ENDOR) at 140 GHz, J. Magn. Reson. 138 (1999) 232–243.

- [9] V. Weis, M. Bennati, M. Rossay, J.A. Bryant, R.G. Griffin, High field DNP and ENDOR with novel multiple-frequency resonance structure, *J. Magn. Reson.* 140 (1999) 293–299.
- [10] B. Epel, D. Arieli, D. Baute, D. Goldfarb, Improving W-band pulsed ENDOR sensitivity—random acquisition and pulsed special TRIPLE, *J. Magn. Reson.* 164 (2003) 78–83.
- [11] J.W.A. Coremans, O.G. Poluektov, E.J.J. Groenen, G.W. Canters, H. Nar, A.J. Messerschmidt, A W-band electron nuclear double resonance study of single crystals of  $^{14}\text{N}$  and  $^{15}\text{N}$  azurin, *J. Am. Chem. Soc.* 118 (1996) 12141–12153.
- [12] D. Arieli, D.E.W. Vaughan, K.G. Strohmaier, D. Goldfarb, High field  $^{31}\text{P}$  ENDOR of  $\text{MnAlPO}_4\cdot 20\text{H}_2\text{O}$ : direct evidence for framework substitution, *J. Am. Chem. Soc.* 121 (1999) 6028–6032.
- [13] A. Pöpl, T. Rudolf, P. Manikandan, D. Goldfarb, A W- and X-band pulsed electron-nuclear double resonance study of a sodium–nitric oxide adsorption complex in NaA zeolite, *J. Am. Chem. Soc.* 122 (2000) 10194–10200.
- [14] R. Grommen, P. Manikandan, Y. Gao, T. Shane, J.J. Shane, R.A. Schoonheydt, B.M. Weckhuysen, D. Goldfarb, Geometry and framework interactions of zeolite-encapsulated copper(II)–histidine complexes, *J. Am. Chem. Soc.* 122 (2000) 11488–11496.
- [15] B. Epel, C.S. Slutter, F. Neese, P.M.H. Kroneck, W.G. Zumft, I. Pecht, Ole Farver, Y. Lu, D. Goldfarb, Electron transfer mediating  $\text{Cu}_4$  centers in proteins: a comparative high field  $^1\text{H}$  ENDOR study, *J. Am. Chem. Soc.* 124 (2000) 8152–8162.
- [16] R.J. Cook, D.H. Whiffen, Relative signs of hyperfine coupling constants by a double ENDOR experiment, *Proc. Phys. Soc.* 84 (1964) 845–848.
- [17] B. Biehl, M. Plato, K. Möbius, General TRIPLE resonance on free radicals in solution. Determination of relative signs of isotropic hyperfine coupling constants, *J. Chem. Phys.* 63 (1975) 3515–3522.
- [18] M. Mehring, P. Höfer, A. Grupp, Pulsed electron nuclear double and triple resonance schemes, *Ber. Bunsenges. Phys. Chem.* 91 (1987) 1132–1137.
- [19] B. Epel, D. Goldfarb, Two-dimensional Pulsed TRIPLE at 95 GHz, *J. Magn. Reson.* 146 (2000) 196–203.
- [20] M. Linder, A. Höhener, R.R. Ernst, Orientation of tensorial interactions determined from 2-dimensional NMR powder spectra, *J. Phys. Chem.* 73 (1980) 4959–4970.
- [21] K. Schmidt-Rohr, H.W. Spiess, *Multidimensional solid state NMR and polymers*, Academic Press, New York, 1994, p. 240.
- [22] G. Jeschke, H.W. Spiess, NMR correlated high-field electron spin resonance spectroscopy, *Chem. Phys. Lett.* 293 (1998) 9–19.
- [23] G.H. Rist, J.S. Hyde, Ligand ENDOR of metal complexes in powders, *J. Chem. Phys.* 52 (1970) 4633–4643.
- [24] B.M. Hoffman, J. Martinsen, R.A. Venters, General theory of polycrystalline ENDOR patterns— $g$  and hyperfine tensors of arbitrary symmetry and relative orientation, *J. Magn. Reson.* 59 (1984) 110–123.
- [25] E. Narr, H. Zimmermann, A. Godt, D. Goldfarb, G. Jeschke, Structure and dynamics of copper complexes with 2,2':6',2''-terpyridines in glassy matrices, *Phys. Chem. Chem. Phys.* 5 (2003) 3959–3967.
- [26] A. Schweiger, G. Jeschke, *Principles of Pulse Electron Paramagnetic Resonance*, Oxford University Press, Oxford, 2001.